PHYSICAL SCIENCES

Topological Fermiology of gate-tunable Rashba electron gases

Jie Hu[1]†, Ze-Zheng Fang[1]†, Feng Sheng[1], Chenqiang Hua[1]*, Chuanying Xi[2], Guangli Kuang[2], Li Pi[2], Kenji Watanabe[3], Takashi Taniguchi[3], Qing-Lin Xia[4]*, Yi Zheng[1,5]*

By introducing first-order quantum phases as topological invariants, recent symmetry analysis–based theories have reinvigorated magnetic quantum oscillations as a versatile quantum probe for unfolding the Fermi surface topology along with the geometry information, i.e., topo-Fermiology. Here, we demonstrate the comprehensive topo-Fermiology of high-mobility Rashba two-dimensional electron gases with ultragate tunability of spin-orbit coupling parameter in few-layer black arsenic. The remarkable consistencies with the key theoretical predictions of period doubling in quantum oscillations, gate-tunable aperiodic beating patterns, and the symmetry-enforced Landau level crossing phenomena controlled by the competition between Rashba coupling and the Zeeman interaction, which ultimately manifests as all odd-filling factor integer quantum Hall effect with superb sensitivity to quantum phases, establish topo-Fermiology as an indispensable methodology for studying topological quantum matters.

INTRODUCTION

The quantization of two-dimensional electron gases (2DEGs) has been a fascinating topic of fundamental research for over five decades, when diverse science frontiers are constantly pioneered by the discovery of unconventional quantization phenomena in emergent 2DEG systems (*1*–*6*). The periodic quantum oscillations of 2DEGs in strong magnetic fields, hallmarking the formation of quantized Landau levels (LLs), provide the most direct and visualized way for resolving the Fermi surface (FS) geometry by measuring the Shubnikov–de Haas oscillations (SdHOs), the de Haas–van Alphen effect, Hall resistance, etc. (*7*). These well-established Fermiology techniques interpret the field-dependent quantum oscillations by the semiclassical Onsager-Lifshitz rule, which directly correlates the FS extrema to the magnetic oscillation frequencies by neglecting the first-order magnetic coupling energy (H_1) (*7*–*9*). Despite the tremendous success, the conventional zeroth-order Fermiology has encountered serious challenges in identifying topological quantum materials, when the prevailing Landau fan diagrams frequently yield sample-dependent or even contradicting results (*10*–*13*). The Landau fan analyses of SdHOs are further plagued by an ambiguity in determining the LL indexes by adopting either oscillation peak maximums or valley minimums and by the coexistence of multiple trivial/nontrivial FSs and the emergence of strong high-harmonic components (*10*, *14*, *15*).

Recently, Alexandradinata *et al.* proposed the topological Fermiology (topo-Fermiology) methodology to systematically probe the topological band parameters along with the FS geometry, based on the Onsager-Lifshitz-Roth quantization theory (*16*–*19*). The key ingredient of this theoretical proposal is the introduction of a first-order quantum phase correction, which unveils the topology of the underlying electronic band structures. Because of H_1-induced symmetry constraints on the quantized cyclotron orbits, the quantum phases can be strictly classified into 10 classes, providing an indispensable quantum probe for determining the topological band parameters. Here, we use gate-tunable high-mobility Rashba 2DEGs in few-layer black arsenic field-effect transistors (bAs FETs) to demonstrate the full power of the topo-Fermiology theory. In the extreme quantum limit, the FS topology of Rashba bands manifests as all odd-filling factor (ν) integer quantum Hall effect (QHE) plateaus, while fine-tuning the Rashba splitting energy toward the high-ν limit enforces drastic quantum phase shifts toward π and a pronounced transition to even-ν QHE plateaus. For fixed Rashba spin-orbit coupling (SOC) parameters, we use magnetic fields as a single parameter to reveal period doubling in the SdHOs, gate-tunable aperiodic beating patterns, and the LL crossing phenomena controlled by the competition of Rashba SOC and the Zeeman energy.

RESULTS AND DISCUSSION

Explicitly, the first-order quantum phase correction λ_a (*16*, *17*) consists of the geometric Berry phase ϕ_B (*20*), the Zeeman phase ϕ_Z, and the orbital magnetic moment phase ϕ_R (*16*, *21*) (see Materials and Methods for the Onsager-Lifshitz-Roth theory and the formulation of λ_a). Under a perpendicular positive gate voltage (V_g), the spin splitting of high-mobility Rashba 2DEGs in few-layer bAs FETs is characterized by a differential area δS between the inner and outer Rashba FSs (Fig. 1A). For weak Zeeman coupling, the dimensionless parameter of $l_B^2\delta S$, where $l_B = \sqrt{\hbar/eB}$ represents the magnetic length, is much larger than the interband magnetic moment of the Bloch wave packets. In this limit, the Onsager-Lifshitz-Roth rule

$$l_B^2 S(k_z, E) + \lambda_a(k_z, E) = 2\pi\left(n + \frac{1}{2}\right) \quad (1)$$

applies to two helical spin-momentum locked Rashba FSs independently, in which case only $\phi_B = \pi$ is relevant to λ_a while the intraband ϕ_Z and ϕ_R are all zero due to the rotation symmetry of the Rashba Hamiltonian (*6*, *18*). By increasing B, the interband

[1]School of Physics and State Key Laboratory of Silicon and Advanced Semiconductor Materials, Zhejiang University, Hangzhou 310027, P. R. China. [2]High Magnetic Field Laboratory, Chinese Academy of Sciences, Hefei 230031, China. [3]National Institute for Materials Science, 1-1 Namiki, Tsukuba 305-0044, Japan. [4]School of Physics and State Key Laboratory of Powder Metallurgy, Central South University, Changsha 410083, P. R. China. [5]Collaborative Innovation Centre of Advanced Microstructures, Nanjing University, Nanjing 210093, P. R. China.
*Corresponding author. Email: huachenqiang@zju.edu.cn (C.H.); qlxia@csu.edu.cn (Q.-L.X.); phyzhengyi@zju.edu.cn (Y.Z.)
†These authors contributed equally to this work.

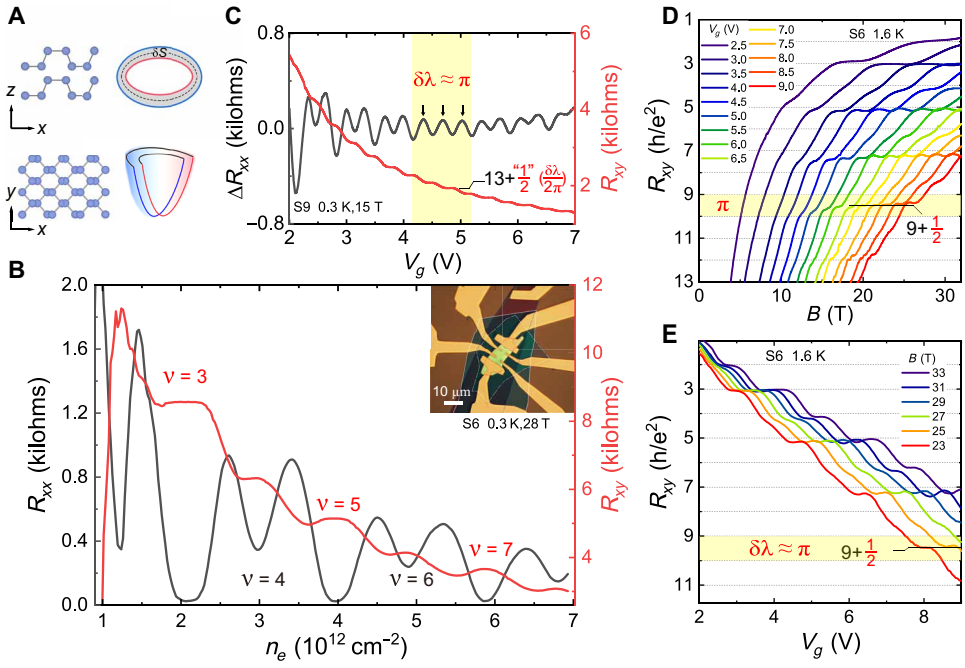

Fig. 1. Integer QHE and gate-tunable quantum phases of bAs Rashba 2DEGs in the extreme quantum limit. (**A**) Left: Centrosymmetric bAs lattice consisting of puckered BP-type monolayers. Right: V_g-tunable Rashba band formations in few-layer bAs by structure inversion asymmetry. (**B**) Integer QHE of bAs high-mobility Rashba 2DEGs, showing all-odd QHE plateaus manifesting the helical spin-momentum locking band topology. Inset: Optical image of FET-S6, where local graphite gate, top hBN, and bottom hBN are outlined by blue, white, and red dashed lines, respectively. (**C**) SdHO of high-mobility FET-S9, exhibiting a conspicuous triple-peak structure in ΔR_{xx} for $\delta\lambda \approx \pi$. In R_{xy}, an anomalous 1/2 shift symbolizes the entry of the $\delta\lambda \approx \pi$ zone but should not be interpreted as fractionally quantized Hall states. (**D**) R_{xy} versus B in the QHE regime for FET-S6 with fixed Δ_R. Note that, for $\delta\lambda = \pi$, all the $\nu = 9$ plateaus show an anomalous shift of 1/2. (**E**) R_{xy} versus V_g in the QHE regime with different B set points, in which the 1/2 plateau shift is well reproduced for $\delta\lambda = \pi$.

hybridization becomes non-negligible, and the quantum phases of gate-tunable Rashba bands will include the SOC term ($l_B^2\delta S$) as well as the interband Zeeman contributions (*18*, *19*)

$$\lambda_{\pm} = \pm\frac{1}{2}\sqrt{\left(l_B^2\delta S\right)^2 + \phi'_Z{}^2} + \pi, \quad \phi'_Z = \pi\left(g'_s\frac{m^*}{m_0} - 2\right) \qquad (2)$$

in which the subscript ±, m^*, and m_0 stand for the outer and inner Rashba FSs, the effective electron mass, and the free electron mass, respectively. Here, ϕ'_Z is referred as the general interband Zeeman phase, in which g'_S is the summation of the interband orbital moment contribution and the conventional Zeeman spin g factor, while the second term under the square root represents the non-Abelian interband Berry phase (*18*, *19*).

The physical meaning of Eq. 2 tells that $\lambda_{\pm}$ are controlled by the competition between the Rashba SOC Δ_R-induced phase $\left(l_B^2\delta S \propto \Delta_R\right)$ and ϕ'_Z (see Materials and Methods), while both FSs have a common π Berry phase originating from the spin-momentum locking band topology. In this hybridization regime with intermediate and small $l_B^2\delta S$ parameters, the inner-outer Rashba FSs become nearly degenerate, quantizing into twofold spin-polarized LLs (*18*, *19*). Following Eq. 1, the resulting ± LLs are characterized by a quantum phase offset of $\delta\lambda = (\lambda_+ - \lambda_-)$ (*18*), which also enforces an LL spin energy splitting of $\Delta E_{\pm} = E_c\delta\lambda/2\pi$ with the cyclotron energy defined by $E_c = \hbar\omega_c$. The correlation between δλ and $\Delta E_{\pm}$ becomes evident by moving λ_a to the right side of Eq. 1, which is essentially the spin-split Landau quantization formula of $E_{\pm} = \left(n + 1/2 + \lambda_{\pm}/2\pi\right)\hbar\omega_c$ with a δλ-dependent spin energy shift of $\Delta E_{\pm}$ (see Materials and Methods for detailed discussions).

For quantum oscillations in few-layer bAs FETs, δλ and ΔE are both gate tunable and B tunable by manipulating Δ_R and ϕ'_Z, respectively. Uniquely, the Rashba energy Δ_R of our bAs 2DEGs can be widely tuned from 0.04 to 1.71 meV by continuously breaking the structure inversion symmetry of bAs channels using a local graphite gate (*6*). In complementary with a 38-T steady magnetic field facility (see Materials and Methods), we are able to widely and continuously tune δλ from the $l_B^2\delta S \gg \phi'_Z$ limit down to the $l_B^2\delta S < \phi'_Z$ regime, which opens the unprecedented possibility to verify the topo-Fermiology theory by either fine-tuning Δ_R with fixed B set points (QHE regime) or by ramping B with gate-tuned Δ_R (SdHO spectroscopy).

As a quantum signature of the helical spin-momentum locked bands, which has a Dirac point at $\mathbf{k} = 0$ due to the time reversal symmetry-enforced Kramers degeneracy, bAs Rashba 2DEGs in the extreme quantum limit show hallmarking all-odd QHE plateaus for vanishing R_{xx}, where Δ_R is less than the Zeeman energy E_Z ($l_B^2\delta S < \phi'_Z$). As shown in Fig. 1B, the R_{xy} plateaus are well defined for $\nu = 3,4,5,6,7$; however, using vanishing R_{xx} as a full-quantization criterion, it is evident that the integer QHE of bAs Rashba 2DEGs is characterized by all-odd filling factors. In stark contrast, for topologically trivial few-layer black phosphorus (BP) with the same puckering square lattice but negligible SOC, the quantization above 30 T is prevailed by the Zeeman effect, producing all-even QHE plateaus (*22*).

Intriguingly, by reducing B set points, there emerges a distinctive triple-peak structure in ΔR_{xx}, i.e., the SdHO amplitude after subtracting a smooth background, when Δ_R is ramped continuously by V_g toward $l_B^2\delta S > \phi'_Z$. As shown in Fig. 1C, for $B = 15$ T, the ϕ'_Z-predominant double-peak structure below $V_g = 4$ V makes a drastic transition into a triple-peak zone, which is followed by reemergent double-peak patterns above $V_g = 5$ V. Considering that E_Z is fixed (*6*), the Zeeman energy splitting of LLs cannot explain the emergence of the triple-peak zone, which is apparently Δ_R dependent. However, by taking the quantum phases of Eq. 2 into account, the V_g-dependent evolution of R_{xx} can be consistently elucidated by the competition of Δ_R and E_Z, which continuously tunes the LL spin splitting energy by $\Delta E_\pm = E_c\delta\lambda/2\pi$. Consequently, the LL spectrum periodically evolves from quasi-degenerate ($\delta\lambda \sim 0$) to equidistant ($\delta\lambda \sim \pi$) when sweeping V_g or B. For the latter, the SdHO peaks are nearly equidistant and show the characteristic destructive interference behavior, i.e., the SdHO beating node. The triple-peak structure corresponds to a $\delta\lambda = \pi$ transition from the ϕ'_Z-predominant regime to $l_B^2\delta S > \phi'_Z$. Such a $\delta\lambda = \pi$ transition controlled by competing Δ_R and E_Z is further confirmed by analyzing the V_g-dependent ΔR_{xx} ratios between the odd-filling and even-filling peaks (*22*). As shown in fig. S5, the $\Delta R_{odd}/\Delta R_{even}$ ratio of the SdHO curve in Fig. 1C monotonically increases by tuning down V_g and becomes large than 1 by crossing the triple-peak zone.

Intriguingly, for Hall resistance R_{xy}, $\delta\lambda = \pi$ manifests as an anomalous 1/2 shift in the QHE plateaus (see Materials and Methods), as indicated in Fig. 1C. However, such an anomalous 1/2 shift also reflects the continuous $\delta\lambda$-dependent evolution in the LL spin splitting energy, which should not be interpreted as fractionally quantized Hall states. The ultrasensitivity of QHE plateaus to $\delta\lambda$, which is not considered by the original theoretical proposal (*17*), makes R_{xy} a superb probe for topo-Fermiology in the extreme quantum limit. In Fig. 1D, we show the evolution of R_{xy} as a function of B for bAs FET-S6 with V_g-set Δ_R. Distinctively, for $\delta\lambda = \pi$, all the $\nu = 9$ R_{xy} plateaus show an anomalous shift of 1/2, which gradually decreases to zero below $\nu = 5$ when the integer QHE takes over. Because $\delta\lambda$ is both V_g and B dependent, we also verify the quantum phase origin of the 1/2 shift by directly measuring R_{xy} in the extreme quantum limit via continuously tuning Δ_R with different B set points. As shown in Fig. 1E, the $\delta\lambda$-shifted QHE plateaus are excellently aligned in energy; however, they shift to lower V_g when B set points are reduced from 33 to 23 T, providing an unambiguous evidence of the interplay between Δ_R and E_Z.

Amazingly, the triple-peak structures symbolizing the $\delta\lambda \approx \pi$ zone are readily observed in the SdHO spectra, in which B-dependent $\delta\lambda$ is predicted to introduce gate-tunable aperiodic beating patterns, oscillation period doubling, and the LL crossing behavior (*18*, *19*). As shown in Fig. 2A, the locations of the prominent triple-peak zone of

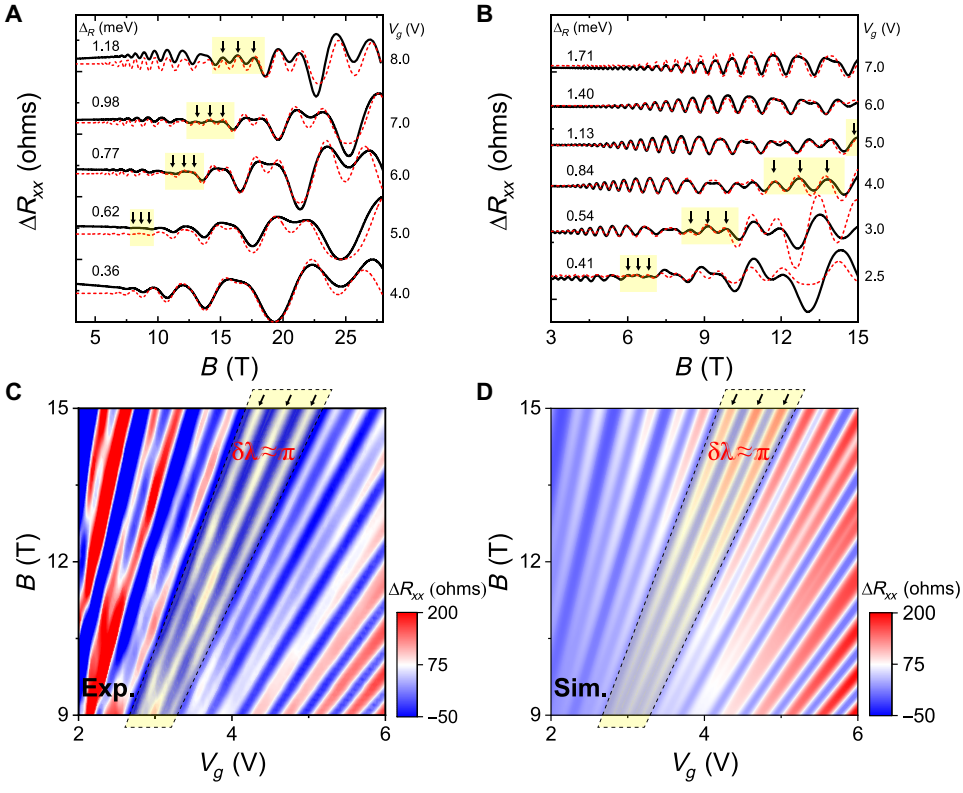

Fig. 2. Aperiodic beating patterns of SdHO with V_g-tunable and B-dependent quantum phases. (**A**) V_g-dependent SdHO of FET-S6, showing that $\delta\lambda \approx \pi$ linearly increases as a function of V_g. The triple-peak feature of $V_g = 5$ V is well resolved on a logarithmic scale, mainly due to the limited measurement resolution of the steady high–magnetic field facility. (**B**) V_g-dependent SdHO of bAs FET-S9, exhibiting the same linear $\delta\lambda \approx \pi$ versus V_g relation. (**C**) 2D mapping of SdHO ΔR_{xx} versus V_g and B for FET-S9, where the triple-peak zone is highlighted by the yellow polygon. Note that the ΔR_{xx} 2D map is collected by sweeping V_g while slow scanning B in steps of 0.1 T. (**D**) Simulation of the experimental 2D map using the spin-polarized SdHO formula.

FET-S6 monotonically shift to higher B values when Δ_R is linearly increased by V_g. The linear dependence of $\delta\lambda = \pi$ on V_g for even lower Δ_R is evident in Fig. 2B, in which FET-S9 exhibits robust SdHOs above 2 T, allowing the low-V_g evolution of $\delta\lambda$ to be fully unfolded using a commercial 15-T cryostat. For Rashba 2DEGs, $\delta\lambda = \pi$ defines the last SdHO beating node, across which E_Z gradually predominates the Rashba SOC because $l_B^2\delta S$ is inversely proportional to B. Thus, the gate-tunable linear growth of the triple-peak structures ($\delta\lambda \approx \pi$) as a function of V_g (Δ_R) compellingly demonstrates the aperiodic beating pattern prediction of the topo-Fermiology theory for Rashba 2DEGs. By identifying the quantum phase origin of the triple-peak structures, we are able to simulate SdHOs as well as the 2D mapping of ΔR_{xx} as a function of both V_g and B by incorporating $\lambda_{\pm}$ into the spin-polarized SdHO formula (*23*) (see Materials and Methods for details). As shown in Fig. 2 (A and B), the simulations capture all the essential features of V_g-dependent SdHO spectra, including the emergence of the triple-peak structure for $\delta\lambda \approx \pi$ followed by the E_Z-controlled double peaks. In Fig. 2 (C and D), we show the outstanding agreement between the experimental mapping data and the simulation results, showing nearly identical SdHO peak positions and the evolution of the triple-peak locations.

The second key prediction of the topo-Fermiology theory for Rashba 2DEGs is the smooth SdHO period doubling in the unit of $1/B$ when B sweeping continuously drives $\delta\lambda$ from 2π to π (*18*). In Fig. 3A, we show a representative SdHO curve with a large Δ_R of 1.18 meV, which requires a large E_Z of $B \sim 14$ T to reach the $\delta\lambda \approx \pi$ zone followed by the extreme quantum limit. After determining $\delta\lambda \approx \pi$, we simulated the SdHO curve by the spin-polarized SdHO formula. The extracted fitting parameters were then used to construct the LL dispersion versus B^{-1} diagrams, in which red and blue lines represent the spin-polarized LLs of the inner and outer Rashba FSs, respectively. As shown in the bottom-left panel of Fig. 3A, at ~6 T, the LLs of FET-S6 is quasi-degenerate when $\delta\lambda$ approaches 2π. By sweeping B toward 28 T, $\delta\lambda$ smoothly decreases until reaching the π zone, where the LLs are quasi-equidistant. Intriguingly, by setting $\Delta_R = 0.01$ meV, we used the same set of fitting parameters to simulate the corresponding SdHO curve in the $l_B^2\delta S \ll \phi'_Z$ limit, which is not experimentally feasible for a steady high–magnetic field facility. As shown in the right panel of Fig. 3A, without the V_g-tunable contributions of $l_B^2\delta S$, the LL dispersions are independent of B and show constant separations between the opposite spin LLs, in excellent agreement with the theoretical work (*18*).

Such a smooth SdHO period doubling phenomenon is intrinsically controlled by the competition between the Rashba SOC and E_Z but not related to sample quality or the absolute magnetic field intensity. In Fig. 3B, we show the analyses of the LL versus B dispersion for FET-S4, which has substantially higher electron mobility than FET-S6 and thus reaches $\delta\lambda = \pi$ at $B \sim 7$ T with a small Δ_R of 0.59 meV. Except that the SdHO starts at a much lower B threshold of ~2 T, the evolution of the B-dependent SdHO periods is essentially the same for both devices. The quantum phase nature of continuous SdHO period doubling is further validated by angle (θ)–dependent SdHO experiments, which effectively reduce E_c while leaving both Δ_R and E_Z unchanged. As shown in Fig. 3C, by plotting SdHO characteristics as a function of both θ and the equivalent out-of-plane magnetic field ($B_\perp$), it is plain to see that the triple-peak structures, i.e., the $\delta\lambda = \pi$ zone, emerge at the same $B_\perp$ values. Such an θ-independent behavior of the $\delta\lambda = \pi$ zone can be well reproduced by the SdHO simulation results, as shown in Fig. 3D.

With the rotational symmetry, the topo-Fermiology theory also predicts robust symmetry-enforced LL crossings in bAs Rashba 2DEGs, when gate-tunable and B-dependent $\delta\lambda$ reverses the energy ordering of the two spin-split Rashba LLs without violating the Wigner–von Neumann "noncrossing rule" (*18*, *24*). Because LL crossings are essentially the manifestation of competing the Rashba SOC and E_Z, the V_g-tunable Δ_R of high-mobility bAs Rashba 2DEGs gives us the unprecedented advantage to test the theoretical proposal by fully exploring $\delta\lambda$ from the $l_B^2\delta S \gg \phi'_Z$ limit down to the $l_B^2\delta S < \phi'_Z$

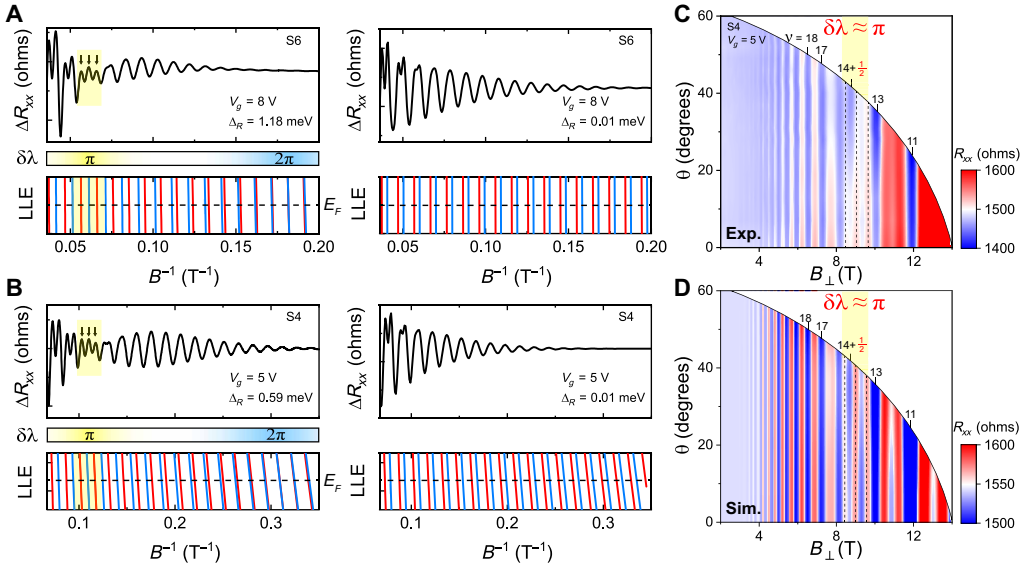

Fig. 3. SdHO period doubling controlled by *B*-dependent quantum phase corrections. (**A**) Continuous SdHO period doubling for FET-S6 with a large Δ_R of 1.18 meV, which requires $B \sim 14$ T to reach the $\delta\lambda \approx \pi$ zone. (**B**) Smooth SdHO period doubling for FET-S4 with $\Delta_R = 0.59$ meV, which pushes the $\delta\lambda \approx \pi$ zone to start at $B \sim 7$ T. (**C**) Angle-dependent 2D mapping of SdHO ΔR_{xx} versus $B_\perp$ for FET-S4. (**D**) Simulation of the 2D ΔR_{xx} map in Fig. 3C with the spin-polarized SdHO formula.

regime. As shown in Fig. 4, for large Δ_R (V_g), a strong SdHO of high-mobility FET-S3 (5000 cm^2 V^{-1} s^{-1}) starts in the $l_B^2\delta S \gg \phi'_Z$ limit and exhibits an extra beating node at ~3.8 T, which corresponds to the $l_B^2\delta S$-dominated $\delta\lambda \approx 3\pi$ regime. By further increasing B, the rapid decrease in $l_B^2\delta S$ monotonically pushes $\lambda\pm$ toward the $l_B^2\delta S < \phi'_Z$ regime, when $\delta\lambda$ produces the 2π beating maxima followed by the triple-peak structures of $\delta\lambda \approx \pi$. As illustrated in Fig. 4B, the continuous 3π-to-π changes in $\delta\lambda$ enforce an LL crossing when spin-↑ and spin-↓ reverse their energy ordering at $B \sim 6$ T ($\delta\lambda \approx 2\pi$). Above 10 T, the ϕ'_Z-predominant double-peak structures prevail, when the Rashba 2DEG approaches the QHE regime. It should be emphasized here that the observed LL crossing phenomena, along with the aforementioned SdHO period doubling and Δ_R-dependent aperiodic beating patterns, are nontrivial and protected by the centrosymmetric bAs lattice (*6*, *18*, *19*).

The amazing experimental verifications of the topo-Fermiology theory based on bAs 2DEGs, a model Rashba system with high carrier mobility and ultragate tunability, call for more systematic topo-Fermiology studies on complex quantum matters with the coexistence of nontrivial and trivial electronic bands. Our results determined that both the inner and outer FSs of bAs Rashba 2DEGs are topologically nontrivial in the QHE regime, as evident by robust $\phi_B = \pi$ for both Rashba orbits, suggesting that the square lattice warping and the associated SOC hierarchic structures (*25*, *26*) play an insignificant role in determining quantum phase corrections. To the best of our knowledge, the anomalous integer QHE of gate-tunable Rashba 2DEGs is also the very first report among 2D materials, providing a tempting platform for exploring unconventional quantization phenomena interwoven with topology. It should also be emphasized that the all-odd quantum Hall plateaus of bAs Rashba 2D hole gases have a rather different origin in the spin-valley symmetry (*6*, *27*).

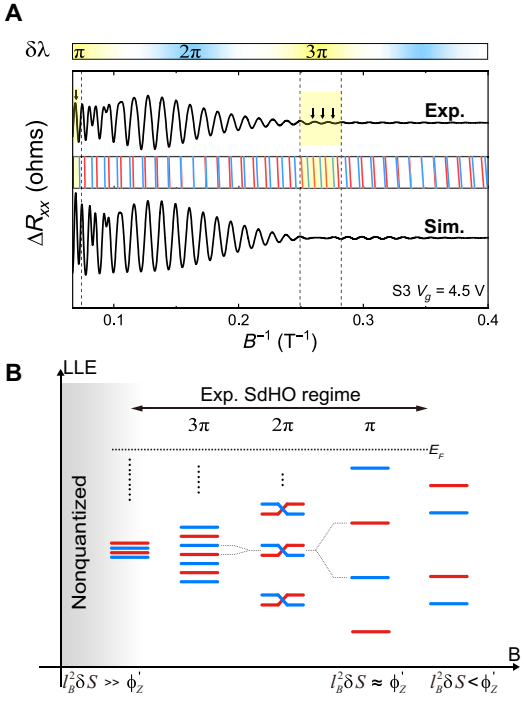

Fig. 4. Symmetry-enforced LL crossings in bAs Rashba 2DEGs. (**A**) Low-V_g SdHO of high-mobility Rashba 2DEGs (bAs FET-S3), allowing ultrawide tuning of the competition between Δ_R and E_Z from the $l_B^2\delta S \gg \phi'_Z$ limit down to the $l_B^2\delta S < \phi'_Z$ regime. Below 5 T, $\delta\lambda$ is dominated by $l_B^2\delta S$, which produces the extra 3π beating node at ~3.8 T. (**B**) Schematic of LL crossings as a function of B. To fully unfold the continuous 3π-to-π changes, large Rashba SOC and high electron mobility are two prerequisites.

MATERIALS AND METHODS

Physical properties of bAs and FET fabrications

BAs is a van der Waals material in which puckered monolayers are AB stacked along the out-of-plane direction, which is referred as the group V analog of the renowned BP (*9*). The centrosymmetric square lattice of bAs belongs to the space group *Cmce* (no. 64), which has a principal twofold rotation axis and a mirror plane perpendicular to the C_2 axis. As constrained by the inversion symmetry and time reversal symmetry, the energy bands of bAs are spin degenerate, unless the structure inversion symmetry is broken by an external gate V_g.

The bAs FETs consisting of bAs/hexagonal boron nitride (hBN)/graphite heterostructures were assembled by the polycarbonate-based dry transfer technique (*28*, *29*), followed by the patterning of Pd/Au (2 and 60 nm, respectively) electrodes by standard electron beam lithography and thermal evaporation technique. In the final step, the prepared FETs were encapsulated by a top hBN layer to finish the device structures of hBN/bAs/hBN/graphite. Detailed information on bAs FET fabrications and basic device characterizations can be found in ref. (*9*).

The Onsager-Lifshitz-Roth quantization theory

The semiclassical Onsager-Lifshitz rule correlates the frequencies of magnetic quantum oscillations to the FS extrema by

$$l_B^2 S(k_z, E) + \gamma = 2\pi n \tag{3}$$

in which $l_B^2 = \hbar / eB$ and $S(k_z, E)$ represent the magnetic length and the FS extrema for cyclotron movement, respectively, while $\gamma = \pi$ is the Maslov phase factor introduced by circular cyclotron orbital movement. Equation 3 is equivalent to the seminal Landau quantization formula of $E_n = (n+1/2)\hbar\omega_c$, considering a parabolic band with $E_F = (\hbar k_F)^2 / m^*$.

By considering higher-order-in-B corrections, the effective Hamiltonian can be expanded in B as

$$H(\mathbf{k}) = H_0(\mathbf{k}) + H_1(\mathbf{k}) + \ \ldots \tag{4}$$

in which $H_0(\mathbf{k})$ is the zeroth-order Peierls-Onsager Hamiltonian for the Onsager-Lifshitz relation. For the $H_1(\mathbf{k})$ correction, this term is linear in B and can be explicitly expressed as (*19*)

$$H_1(\mathbf{k}) = -\mathbf{B} \cdot \mathbf{M}(\mathbf{k}), \text{ in which} \tag{5}$$

$$\mathbf{M}(\mathbf{k}) = -\frac{g_s}{2}\frac{|e|}{m_e c}\mathbf{S} - \frac{|e|}{2c}\left(\mathbf{r}_{\text{off}} \times \mathbf{v}_{\text{off}} + \mathbf{r}_{\text{intra}} \times \mathbf{v}_{\text{intra}}\right) \tag{6}$$

The three terms of $\mathbf{M}(\mathbf{k})$ in Eq. 6 correspond to the conventional Zeeman coupling, the orbital magnetic moments, and the non-Abelian Berry phases, respectively (*17*, *19*). It is also noteworthy that the last two terms include both intraband and interband contributions when interorbital hybridization is non-negligible (*17*, *19*).

By taking the first-order magnetic field coupling into account, the Onsager-Lifshitz-Roth quantization theory becomes

$$l_B^2 S(k_z, E) + \gamma + \lambda_a(k_z, E) = 2\pi n \quad (7)$$

where $\lambda_a(k_z, E)$ is the quantum phase corrections encoding the topological band parameters, and the subscript index a represents the LL degeneracy. Explicitly, $\lambda_a(k_z, E)$ is contributed by three first-order coupling terms

$$\lambda_a(k_z, E) = \phi_B + \phi_Z + \phi_R \quad (8)$$

in which ϕ_B, ϕ_Z, and ϕ_R are the Berry geometric phase, the Zeeman phase, and the orbit magnetic momentum phase, respectively.

To see the critical role of λ_a on determining the QHE and SdHO, it is convenient to move γ and λ_a to the right side of Eq. 7

$$l_B^2 S(k_z, E) = 2\pi\left(n + \frac{1}{2} + \frac{\lambda_a}{2\pi}\right) \quad (9)$$

From Eq. 9, it is clear that the H_1-induced λ_a will not only introduce an extra phase shift to the SdHO spectra but also enforce an LL energy splitting of $\Delta E = E_c\delta\lambda/2\pi$. For the special case of $\delta\lambda = \pi$, all LLs are shifted by 1/2, which explains the anomalous quantum Hall plateaus when V_g tunes bAs Rashba 2DEGs out of the extreme quantum limit.

For nearly degenerate Rashba bands ($\delta S/S \ll 1$), the quantum phases of the cyclotron orbits of spin-momentum locked quasiparticles can be solved in the energy basis of the Rashba Hamiltonian

$$\lambda_\pm = \pm\frac{1}{2}\sqrt{\left(l_B^2\delta S\right)^2 + \pi^2\left(g_s\frac{m^*}{m_0} - 2\right)^2} + \pi \quad (10)$$

The second quantity under the square root in Eq. 10 represents the general Zeeman phase (ϕ'_Z), which includes both ϕ_Z and the interband geometric Zeeman interaction introduced by field-induced hybridization between the Rashba SOC split orbits. In the strong hybridization limit of $l_B^2\delta S \ll \phi'_Z$, $\delta\lambda = 2\,|\,\lambda_\pm\,| = \pi g_s m^*/m_0$, which corresponds exactly to the well-known Zeeman energy of $E_Z = g_s\mu_B B$ for LL spin degeneracy splitting in the absence of Rashba SOC.

SdHO simulations with topological quantum phase corrections

We carried out the spin-polarized SdHO simulations based on analyzing the two pocket magnetoresistivity of a nearly degenerate Rashba 2DEG system (*23*). By including the topological quantum phase corrections, the LL energy is spin split by an energy of $\Delta E = \hbar\omega_c\delta\lambda/2\pi$. Following Eq. 10, the corrected LL energy spectrum of nearly degenerate Rashba bands can be rewritten as follows

$$\begin{aligned} E_n^\pm &= \left(n + \frac{1}{2}\right)\hbar\omega_c \pm \frac{1}{2}\hbar\omega_c\delta\lambda/2\pi \\ &= \hbar\omega_c\left[n \pm \frac{1}{2}\sqrt{\left(g_s\frac{m^*}{2m_0} - 1\right)^2 + n\frac{\Delta_R^2}{E_F\hbar\omega_c}}\right] \end{aligned} \quad (11)$$

where the Fermi energy E_F is a tunable parameter for generating the LL dispersion, and Δ_R correlates to δS by $\Delta_R = \frac{\hbar^2}{2\pi m^*}\delta S$. It is clear that $E_n^\pm$ represents the energy of the nth LLs with spin up (+) and spin down (−), respectively. In the strong hybridization limit, $\delta\lambda = \pi g_s m^*/m_0$ and thus $E_n^\pm = E_n \pm \frac{\delta\lambda}{2\pi}\hbar\omega_c = \left(n + \frac{1}{2}\right)\hbar\omega_c \pm \frac{1}{2}g_s\mu_B B$, which corresponds to the LL spin degeneracy splitting by the Zeeman coupling.

For a Rashba 2DEG at 0 K, the magnetoconductance can be expressed as (*23*)

$$\sigma_{xx} \propto \sum_{n\pm}\left(n \pm \frac{1}{2}\right)\exp\left[-\frac{\left(E_F - E_n^\pm\right)^2}{\Gamma_0^2}\right] \quad (12)$$

in which $\Gamma_0 = \hbar eB_{\mathrm{SdH}}/m^*$ represents the LL broadening, and the spin-polarized LL energy $E_n^\pm$ encodes the quantum phase offsets. Here, B_{SdH} is the critical field at which SdHOs emerge. For a quantized 2DEG, magnetoresistivity ρ_{xx} is given by

$$\rho_{xx} = \frac{\sigma_{xx}}{\sigma_{xx}^2 + \sigma_{xy}^2} \approx \frac{\sigma_{xx}}{\sigma_{xy}^2} \approx \sigma_{xx}\left(\frac{B}{en}\right)^2 \quad (13)$$

where the prerequisite of $\sigma_{xy} \geq \sigma_{xx}$ is satisfied for most of the SdHO regime. Using Eq. 13, we can readily extract the V_g-dependent and B-dependent quantum phase contributions by analyzing the spin-polarized SdHO of bAs Rashba 2DEGs.

Note that, to make the experimental verifications of the topo-Fermiology theory more reliable, we have adopted a single parameter (Δ_R) approach for the R_{xx} fitting. Despite the simplicity, the simulations of R_{xx} capture all the essential features such as the evolution of the triple-peak structures with V_g and B and the double-peak structures away from the $\delta\lambda \sim \pi$ zone.

Quantum transport measurements

SdHOs and V_g-dependent and B-dependent R_{xx} and R_{xy} were measured with multiple SR830 lock-in amplifiers using a typical excitation current of 100 nA at 13.33 Hz. The gate voltage was supplied by a Keithley 2400 source-measure meter. The He_3 temperature quantum transport measurements were performed using a home-made insert in the 38-T steady magnetic field end-station of the High Magnetic Field Laboratory of Chinese Academy of Sciences (CAS). A 14-T TeslatronPT Cryofree system (Oxford Instruments) was used to measure the SdHO of high-mobility FET S3, S4, and S9 and angle-dependent R_{xx} of FET-S4. Regarding the direction of magnetic field, we mounted the samples on a ceramic leadless chip carrier, which can be rotated in situ by ±100° with reference to the magnetic field, and a Hall sensor is attached to the socket for calibrating θ.

Supplementary Materials

This PDF file includes:

Supplementary Text
Figs. S1 to S9

REFERENCES AND NOTES

1. K. von Klitzing, G. Dorda, M. Pepper, New method for high-accuracy determination of the fine-structure constant based on quantized Hall resistance. *Phys. Rev. Lett.* **45**, 494–497 (1980).
2. D. C. Tsui, H. L. Stormer, A. C. Gossard, Two-dimensional magnetotransport in the extreme quantum limit. *Phys. Rev. Lett.* **48**, 1559–1562 (1982).
3. K. S. Novoselov, A. K. Geim, S. V. Morozov, D. Jiang, M. I. Katsnelson, I. V. Grigorieva, S. V. Dubonos, A. A. Firsov, Two-dimensional gas of massless Dirac fermions in graphene. *Nature* **438**, 197–200 (2005).
4. Y. Zhang, Y.-W. Tan, H. L. Stormer, P. Kim, Experimental observation of the quantum Hall effect and Berry's phase in graphene. *Nature* **438**, 201–204 (2005).

5. C.-Z. Chang, J. Zhang, X. Feng, J. Shen, Z. Zhang, M. Guo, K. Li, Y. Ou, P. Wei, L.-L. Wang, Z.-Q. Ji, Y. Feng, S. Ji, X. Chen, J. Jia, X. Dai, Z. Fang, S.-C. Zhang, K. He, Y. Wang, L. Lu, X.-C. Ma, Q.-K. Xue, Experimental observation of the quantum anomalous Hall effect in a magnetic topological insulator. *Science* **340**, 167–170 (2013).
6. F. Sheng, C. Hua, M. Cheng, J. Hu, X. Sun, Q. Tao, H. Lu, Y. Lu, M. Zhong, K. Watanabe, T. Taniguchi, Q. Xia, Z.-A. Xu, Y. Zheng, Rashba valleys and quantum Hall states in few-layer black arsenic. *Nature* **593**, 56–60 (2021).
7. D. Shoenberg, *Magnetic Oscillations in Metals* (Cambridge Univ. Press, 1984).
8. L. Onsager, Interpretation of the de Haas-van Alphen effect. *Philos. Mag.* **43**, 1006–1008 (1952).
9. I. M. Lifshitz, A. M. Kosevich, Theory of magnetic susceptibility in metals at low temperature. *Sov. Phys. JETP* **2**, 636–645 (1956).
10. Z. Wang, Y. Zheng, Z. Shen, Y. Lu, H. Fang, F. Sheng, Y. Zhou, X. Yang, Y. Li, C. Feng, Z.-A. Xu, Helicity protected ultrahigh mobility Weyl fermions in NbP. *Phys. Rev. B* **93**, 121112 (2016).
11. J. Klotz, S.-C. Wu, C. Shekhar, Y. Sun, M. Schmidt, M. Nicklas, M. Baenitz, M. Uhlarz, J. Wosnitza, C. Felser, B. Yan, Quantum oscillations and the Fermi surface topology of the Weyl semimetal NbP. *Phys. Rev. B* **93**, 121105 (2016).
12. C. Schindler, D. Gorbunov, S. Zherlitsyn, S. Galeski, M. Schmidt, J. Wosnitza, J. Gooth, Strong anisotropy of the electron-phonon interaction in NbP probed by magnetoacoustic quantum oscillations. *Phys. Rev. B* **102**, 165156 (2020).
13. J. Wang, J. Niu, B. Yan, X. Li, R. Bi, Y. Yao, D. Yu, X. Wu, Vanishing quantum oscillations in Dirac semimetal $ZrTe_5$. *Proc. Natl. Acad. Sci. U.S.A.* **115**, 9145–9150 (2018).
14. G. Qiu, C. Niu, Y. Wang, M. Si, Z. Zhang, W. Wu, P. D. Ye, Quantum Hall effect of Weyl fermions in n-type semiconducting tellurene. *Nat. Nanotechnol.* **15**, 585–591 (2020).
15. C. Guo, A. Alexandradinata, C. Putzke, A. Estry, T. Tu, N. Kumar, F.-R. Fan, S. Zhang, Q. Wu, O. V. Yazyev, K. R. Shirer, M. D. Bachmann, H. Peng, E. D. Bauer, F. Ronning, Y. Sun, C. Shekhar, C. Felser, P. J. W. Moll, Temperature dependence of quantum oscillations from non-parabolic dispersions. *Nat. Commun.* **12**, 6213 (2021).
16. L. M. Roth, Semiclassical theory of magnetic energy levels and magnetic susceptibility of Bloch electrons. *Phys. Rev.* **145**, 434–448 (1966).
17. A. Alexandradinata, C. Wang, W. Duan, L. Glazman, Revealing the topology of Fermi-surface wave functions from magnetic quantum oscillations. *Phys. Rev. X* **8**, 011027 (2018).
18. C. Wang, W. Duan, L. Glazman, A. Alexandradinata, Landau quantization of nearly degenerate bands and full symmetry classification of Landau level crossings. *Phys. Rev. B* **100**, 014442 (2019).
19. A. Alexandradinata, L. Glazman, Fermiology of topological metals. *Annu. Rev. Condens. Matter Phys.* **14**, 261–309 (2023).
20. M. V. Berry, Quantal phase factors accompanying adiabatic changes. *Proc. R. Soc. London Ser. A Math. Phys. Sci.* **392**, 45–47 (1984).
21. M.-C. Chang, Q. Niu, Berry phase, hyperorbits, and the Hofstadter spectrum: Semiclassical dynamics in magnetic Bloch bands. *Phys. Rev. B* **53**, 7010–7023 (1996).
22. L. Li, F. Yang, G. J. Ye, Z. Zhang, Z. Zhu, W. Lou, X. Zhou, L. Li, K. Watanabe, T. Taniguchi, K. Chang, Y. Wang, X. H. Chen, Y. Zhang, Quantum Hall effect in black phosphorus two-dimensional electron system. *Nat. Nanotechnol.* **11**, 593–596 (2016).
23. B. Das, S. Datta, R. Reifenberger, Zero-field spin splitting in a two-dimensional electron gas. *Phys. Rev. B* **41**, 8278–8287 (1990).
24. J. V. Neumann, E. Wigner, *Quantum Chemistry: Classic Scientific Papers* (World Scientific, 2000).
25. L. Bawden, J. M. Riley, C. H. Kim, R. Sankar, E. J. Monkman, D. E. Shai, H. I. Wei, E. B. Lochocki, J. W. Wells, W. Meevasana, T. K. Kim, M. Hoesch, Y. Ohtsubo, P. Le Fèvre, C. J. Fennie, K. M. Shen, F. Chou, P. D. C. King, Hierarchical spin-orbital polarization of a giant Rashba system. *Sci. Adv.* **1**, e1500495 (2015).
26. H. Lu, Z. Qi, Y. Huang, M. Cheng, F. Sheng, Z. Deng, S. Chen, C. Hua, P. He, Y. Lu, Y. Zheng, Unlocking hidden spins in centrosymmetric 1*T* transition metal dichalcogenides by vacancy-controlled spin-orbit scattering. *Phys. Rev. B* **107**, 165419 (2023).
27. X. Li, F. Zhang, Q. Niu, Unconventional quantum Hall effect and tunable spin Hall effect in Dirac materials: Application to an isolated MoS_2 trilayer. *Phys. Rev. Lett.* **110**, 066803 (2013).
28. L. Wang, I. Meric, P. Y. Huang, Q. Gao, Y. Gao, H. Tran, T. Taniguchi, K. Watanabe, L. M. Campos, D. A. Muller, J. Guo, P. Kim, J. Hone, K. L. Shepard, C. R. Dean, One-dimensional electrical contact to a two-dimensional material. *Science* **342**, 614–617 (2013).
29. P. J. Zomer, M. H. D. Guimarães, J. C. Brant, N. Tombros, B. J. van Wees, Fast pick up technique for high quality heterostructures of bilayer graphene and hexagonal boron nitride. *Appl. Phys. Lett.* **105**, 013101 (2014).

Acknowledgments

Funding: This work is supported by the National Science Foundation of China (grant nos. 12374194 and 12274467), Zhejiang Provincial Natural Science Foundation (grant no. D19A040001), and the National Key R&D Program of the MOST of China (grant no. 2023YFA1406302). The main part of this work was performed on the Steady High Magnetic Field Facilities, High Magnetic Field Laboratory of CAS, and Y.Z. acknowledges support from the Users with Excellence Project of Hefei Science Center CAS (2021HSC-UE007). The project was also supported by the State Key Laboratory of Powder Metallurgy, Central South University, Changsha, China. We appreciate Z. H. Liu of Longde Group Ltd. for providing natural bAs crystals. **Author contributions:** Y.Z. initiated and supervised the project. J.H., Z.-Z.F., and F.S. fabricated bAs devices and carried out all the measurements, with assistance from C.X., G.K., and L.P. for high–magnetic field experiments. C.H. did the DFT calculations. K.W. and T.T. prepared high-quality hBN single crystals. J.H., Z.-Z.F., C.H., Q.-L.X., and Y.Z. analyzed the data and wrote the paper with inputs from all authors. **Competing interests:** The authors declare that they have no competing interests. **Data and materials availability:** All data needed to evaluate the conclusions in the paper are present in the paper and/or the Supplementary Materials.

Submitted 13 April 2024
Accepted 17 October 2024
Published 20 November 2024
10.1126/sciadv.adp8208